A Total-Variation Compressive Sensing Approach for the Design of Linear Clustered Arrays

N. Anselmi, G. Gottardi, G. Oliveri, and A. Massa

Abstract

In this work, an innovative methodology for the design of *physically-contiguous* clustered linear arrays is proposed. The developed approach is based on a *sparseness-promoting* method based on a total-variation compressive sensing (*TV-CS*) solver. Thanks to the adopted formulation, the design of the array feeding network is achieved by maximizing the sparsity of the gradient of the excitations subject to the matching of user-defined far-field pattern features. A preliminary numerical example is provided to verify the effectiveness of the proposed method when dealing with the design of a clustered linear array yielding a Taylor pattern with predefined side-lobe level.

Contents

1 Introduction

The use of digital beam-forming networks (BFNs) in phased array antennas allows a real-time electronic control of the beam, enabling a set of advanced attractive functionalities such as beam shaping, fast beam scanning, and multiple digital beams sensing [1]. However, their high implementation cost has limited the use of phased array systems, which have been mainly adopted in military and space applications. For such a reason, *unconventional* architectures, such as sparse, thinned and clustered arrays, have been recently proposed [1]. In this framework, clustered phased array architectures are nowadays a good compromise between antenna radiation performance and implementation costs. As a matter of fact, they allow to reduce the total number of transmission/receive (T/R) modules of the BFN, which are known to have a significant impact on the final cost of the antenna. One of the main drawback of this type of architectures is represented the high quantization lobes, getting higher and higher as the number of sub-arrays is lower and lower with respect to the number of original radiating elements. It has been shown that the periodicity introduced by uniform clustering on the aperture illumination quantization is the main reason of the side-lobe level (SLL) degradation. To overcome such an issue, non uniform clustering methods have been proposed in the last years [1].

2 Mathematical Formulation

Let us consider the synthesis of a linear array with a prescribed radiated pattern, whose N elements are uniformly displaced along the x-axis and grouped into contiguous sub-arrays controlled by $C < N$ T/R modules [Fig. 1(a)].
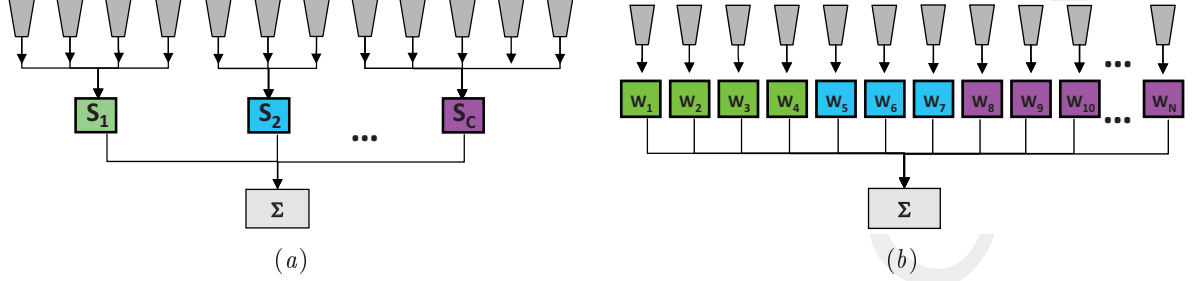

Figure 1: (a) Physical linear clustered array consisting of C sub-arrays and (b) equivalent ("logical") layout.

The synthesis problem at hand can be formulated as follows

Linear Array Clustering Problem: find the array excitations w_n, $n = 1, ... N$, of the equivalent "logical" layout [Fig. 1(b)] having the lowest possible number of clusters, C, and satisfying the pattern matching condition

$$\sum_{k=1}^{K} \left| F_{ref}(u_k) - \sum_{n=1}^{N} w_n e^{j2\pi n d u_k} \right|^2 \leq \epsilon \qquad (1)$$

where F_{ref} is a user-defined reference pattern, d is the inter-element spacing, $u_k = \sin(\theta_k)$, $k = 1, ..., K$, are K angular samples, and ϵ is the tolerance threshold of the pattern matching condition.

The unknown excitations vector $\mathbf{w} = \{w_n; n = 1, ..., N\}$ is related to the corresponding radiated pattern by means of the following expression

$$\mathbf{F}_{REF} = \Phi \mathbf{w} \qquad (2)$$

where $\mathbf{F}_{REF} = \{F_{REF}(u_k); k = 1, ..., K\}$, and Φ is the "observation matrix"

$$\Phi \triangleq \begin{bmatrix} \exp(j2\pi d u_1) & \cdots & \exp(j2\pi N d u_1) \\ \vdots & \ddots & \vdots \\ \exp(j2\pi d u_K) & \dots & \exp(j2\pi N d u_K) \end{bmatrix}. \qquad (3)$$

The vector $\mathbf{w}$ contains the N equivalent excitations coefficients [Fig. 1(b)] expressed as follows

$$w_n = \sum_{c=1}^{C} S_c \delta_{q_n}^{(c)} = \sum_{c=1}^{C} \alpha_c e^{j\beta_c} \delta_{q_n}^{(c)}; \quad n = 1, ..., N \qquad (4)$$

where $S_c = \alpha_c e^{j\beta_c}$ is the complex excitation associated of the cth sub-array [$c = 1, ..., C$ - Fig. 1(a)], α_c and β_c being the amplifier and phase shifter/time-delay, respectively, and $\delta_{q_n}^{(c)}$ is the Kronecker delta function that

defines the clustering of the array elements, i.e.,

$$
\delta_{q_n}^{(c)} = \begin{cases} 1 & \text{if} \quad q_n = c \\ 0 & \text{otherwise} \end{cases}
\tag{5}
$$

$q_n \in [1, C]$, $n = 1, ..., N$, being a set of integer values that univocally defines the sub-arrays of the clustering configuration (i.e., each q_n identifies the cluster to which the n-th element belongs).

According to (4), it is worth noticing that if $C < N$ and only contiguous clusters are allowed, meaning that the vector $\mathbf{w}$ is a piece-wise constant function [Fig. 2(a)]. Accordingly, the gradient of $\mathbf{w}$, defined as [17]

$$
\bigtriangledown \mathbf{w} = \left\{ \bigtriangledown w_n = (w_{n-1} - w_n); \quad n = 1, ..., N \right\}
\tag{6}
$$

turns out to be non-null only for elements indexes n that belongs to two different contiguous clusters [the periodic boundary condition $w_{n-1}|_{n=0} = w_{n-1}|_{n=N}$ is considered in (6) [17]]. The vector $\bigtriangledown \mathbf{w}$ is thus *sparse* [Fig. 2(b)], enabling the use of a CS strategy for finding the problem solution.
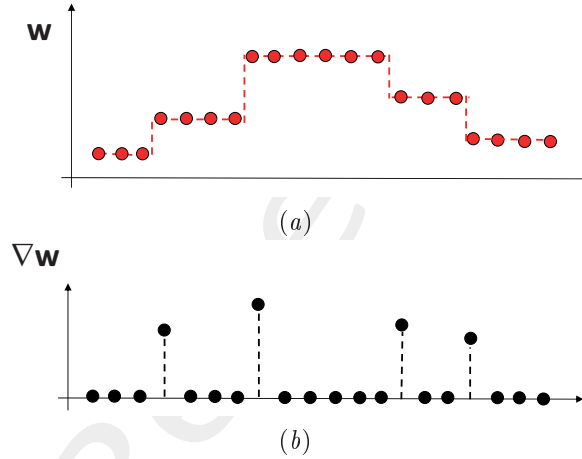

Figure 2: (a) Piece-wise clustered excitations and (b) corresponding (sparse) gradient function.

Accordingly, the clustering problem can be reformulated as a $TV - CS$ synthesis one as follows

$$
\mathbf{w}^{TV-CS} = \arg \left\{ \min_{\mathbf{w}} \left[|\bigtriangledown \mathbf{w}|_1 \right] \right\}, \text{ s.t. } \mathbf{F}_{REF} = \Phi \mathbf{w}
\tag{7}
$$

where $|\cdot|_1$ is the l_1-norm operator. In (7) the minimization of the number of clusters, C, is obtained by searching for the sparsest $\bigtriangledown \mathbf{w}$ vector (i.e., by minimizing the l_1-norm TV term) satisfying the requirement of the pattern matching condition. In order to solve the $TV - CS$ sparse problem (7), the deterministic alternating direction algorithm has been applied [17].

The step-wise behaviour of the vector $\mathbf{w}^{TV-CS}$ allows to define C contiguous clusters composed by one element and/or grouping two or more elements. Accordingly, the clustering coefficients q_n, $n = 1, ..., N$, are obtained by "filtering" the $\mathbf{w}^{TV-CS}$ vector such that two contiguous clusters control points differ at least by a tolerance

factor τ_c. The clustering coefficients are thus obtained as follows

$$
\begin{aligned}
q_1 &= 1 \\
q_n &= \begin{cases} q_{n-1} & \text{if } |\alpha_n - \alpha_{n-1}| < \tau_c \\ q_{n+1} + 1 & \text{otherwise} \end{cases} \quad ; \; n = 2, ..., N.
\end{aligned}
\tag{8}
$$

This means that if two contiguous elements are associated to $\mathbf{w}^{TV-CS}$ values whose difference is less than τ_c, the two elements are grouped together into the same cluster. Finally, the equivalent excitations w_n and the radiated pattern $F(u)$ are obtained using (4) and (2), respectively, and the $TV - CS$ solution "quality" is evaluated by means of the following pattern matching index

$$
\xi = \frac{\int_{-1}^{1} | F_{REF}(u) - F(u) |^2 \, du}{\int_{-1}^{1} | F_{REF}(u) |^2 \, du}
\tag{9}
$$

3 Preliminary Numerical Results

3.1 Taylor - $SLL = -20dB$ - $N = 100$

Array Geometry:

- Linear Array

- Number of Elements: $N = 100$

- Element Spacing: $\Delta L_{REF} = \lambda/2$

- Aperture Length: $L = 49.5\lambda$

Reference Pattern:

- Pencil Beam, Taylor

- Number of elements: $N = 100$

- Transition Index: $\overline{n} = 6$

- Sidelobe Ratio: $SLL = -20dB$

Pareto Parameters:

- Pattern Samples: $K \in \{4, 6, 8..., 20, 25, ..., 50, 60, 70, ..., 100, 300, 400, 500, 1000\}$

- Primary penalty parameter: $\mu \in \left\{2 \times 10^{-2}, 2 \times 10^{-1}, ..., 2 \times 10^{13}\right\}$

- Secondary penalty parameter: $\beta \in \left\{2 \times 10^{-2}, 2 \times 10^{-1}, ..., 2 \times 10^{13}\right\}$

- $m_t \in \left\{1 \times 10^1, 2 \times 10^1, 5 \times 10^1, 1 \times 10^2, 5 \times 10^2, 1 \times 10^3\right\}$

TV-CS Parameters:

- Starting primary penalty parameter: $\mu_0 = \mu$ (default)

- Starting secondary penalty parameter: $\beta_0 = \beta$ (default)

- Outer stopping tolerance: $t_o = 1 \times 10^{-3}$ (default)

- Inner stopping tolerance: $t_i = 1 \times 10^{-3}$ (default)

- Outer maximum iterations: $m_o = 10$ (default)

- Isotropic/anisotropic TV flag: $\mathcal{F}_{TV} = 1$

- Negative/Positive signal: $\mathcal{F}_N = [false]$ (default)

- TV/L2 flag: $\mathcal{F}_{T2} = [false]$ (default)

- Real/Imaginary signal flag: $\mathcal{F}_R = [false]$ (default)

- Scaling Matrix A flag: $\mathcal{F}_A = [true]$ (default)

- Scaling Vector B flag: $\mathcal{F}_B = [true]$ (default)

- Guess Solution: $\mathcal{F}_G = 0$ (all zeroes)

RESULTS - TOLERANCE: $\tau_C = 1.0 \times 10^{-3}$
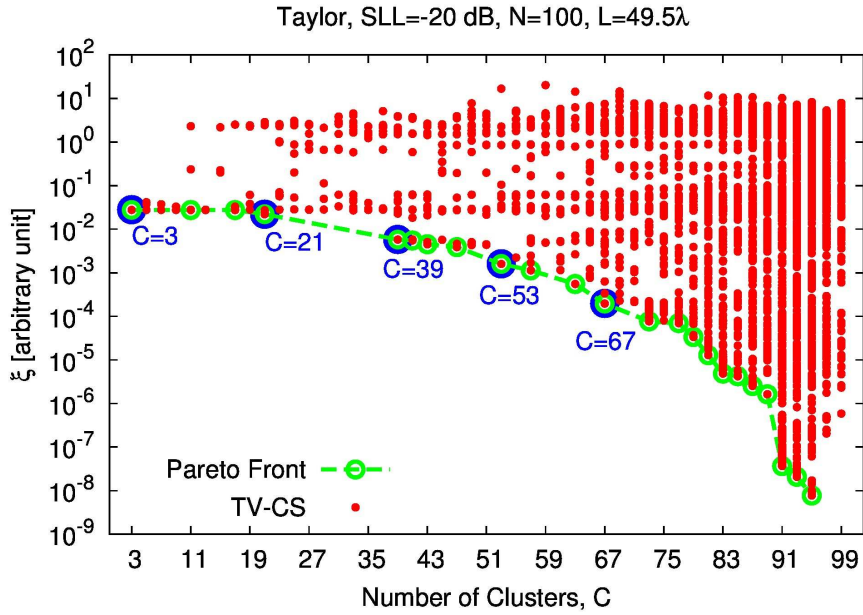
Pareto Front:

Figure 3: *Performance Assessment (Taylor Pattern, $N = 100$, $SLL = -20$ dB, $d = 0.5\lambda$, $L == 49.5\lambda$)*$-$Pareto front.

C	ξ	μ	β	K	m_t	m_o
3	2.76×10^{-2}	1×10^0	2×10^8	35	1×10^3	1×10^1
21	2.20×10^{-2}	2×10^{-1}	$2 \times 10^{+6}$	100	1×10^3	1×10^1
39	5.78×10^{-3}	2×10^0	2×10^5	100	1×10^3	1×10^1
53	1.59×10^{-3}	2×10^0	2×10^3	200	1×10^3	1×10^1
67	1.97×10^{-4}	2×10^0	2×10^2	1000	1×10^2	1×10^1

Table I: *Performance Assessment (Taylor Pattern, $N = 100$, $SLL = -20$ dB, $d = 0.5\lambda$, $L = 49.5\lambda$)*$-$Selected solutions.
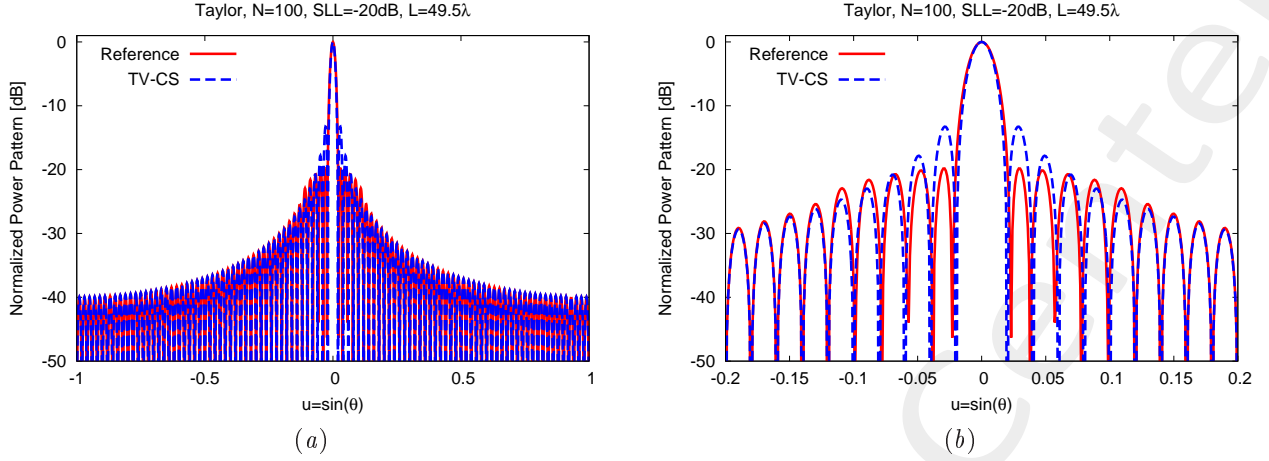
Number of Clusters: $C = 3$

Figure 4: *Performance Assessment* (*Taylor Pattern*, $N = 100$, $SLL = -20$ dB, $d = 0.5\lambda$, $L = 49.5\lambda$, $C = 3$)--Power pattern over the whole visible $u-$range (a) and a detail of the main lobe (b).
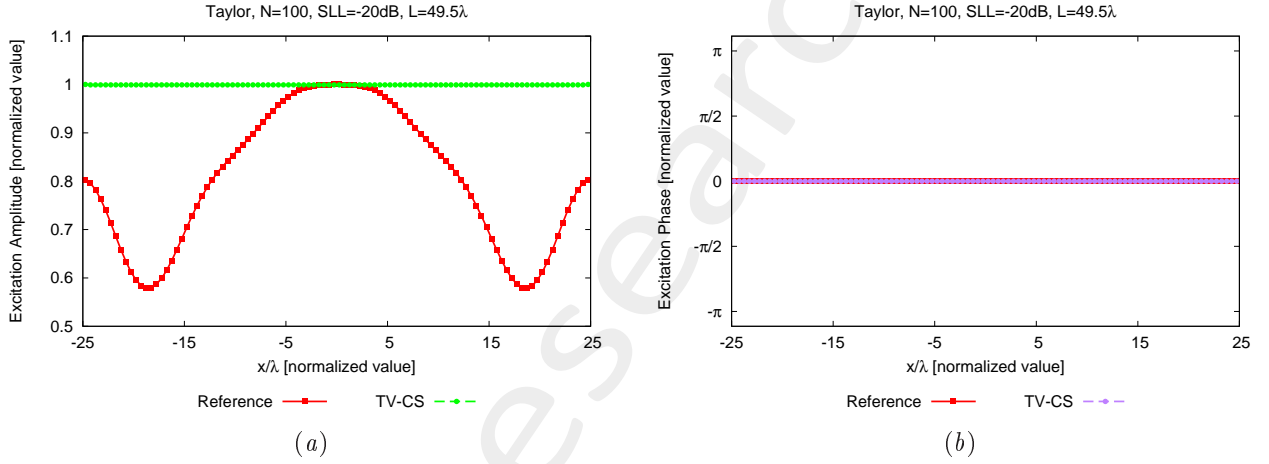

Figure 5: *Performance Assessment* (*Taylor Pattern*, $N = 100$, $SLL = -20$ dB, $d = 0.5\lambda$, $L = 49.5\lambda$, $C = 3$)--Excitations amplitude (a) and phase (b).
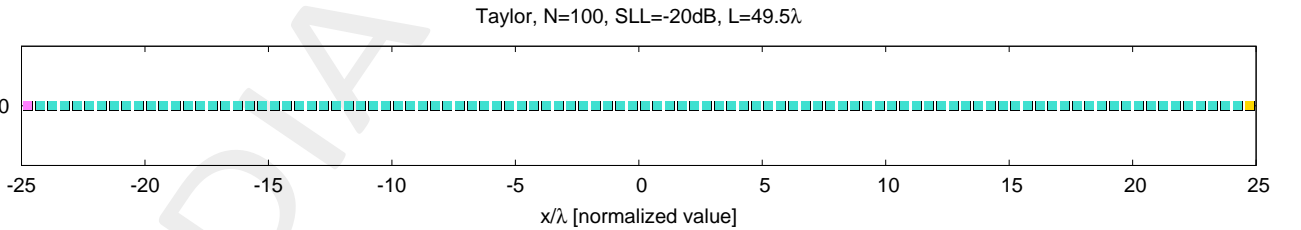

Figure 6: *Performance Assessment* (*Taylor Pattern*, $N = 100$, $SLL = -20$ dB, $d = 0.5\lambda$, $L = 49.5\lambda$, $C = 3$)--Array elements clustering configuration.

	C	SLL [dB]	BW [deg]	$D_{\max}$ [dB]	DRR_{max}[dB]	$\xi\ [\times 10^{-2}]$
Reference	$-$	-19.82	1.0842	19.87	2.37	$-$
$TV-CS$	3	-13.28	1.0124	20.00	3.8×10^{-3}	2.76

Table II: *Performance Assessment* (*Taylor Pattern*, $N = 100$, $SLL = -20$ dB, $d = 0.5\lambda$, $L = 49.5\lambda$, $C = 3$)--Array Performance Indexes.
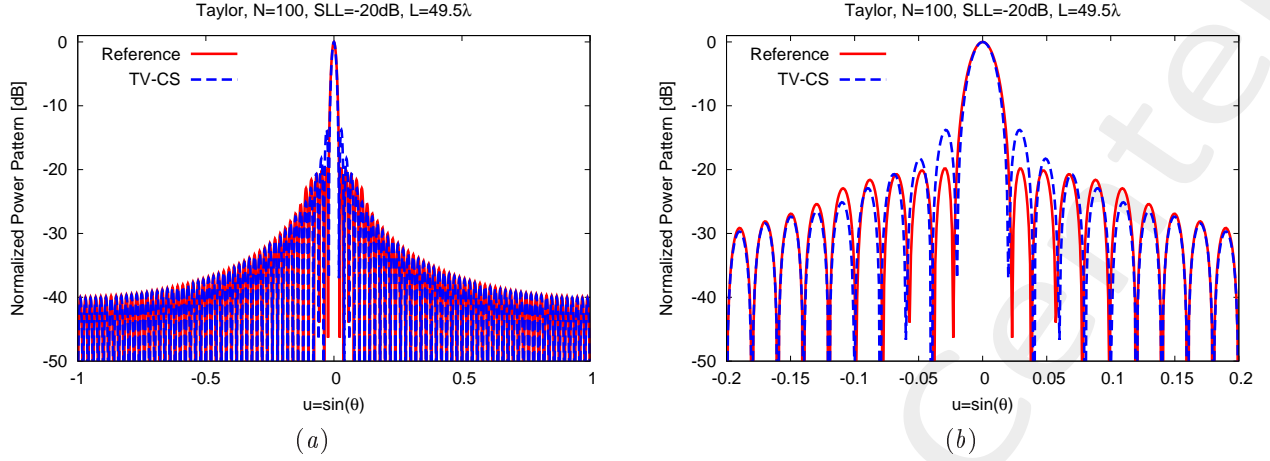
Number of Clusters: $C = 21$

Figure 7: *Performance Assessment* (*Taylor Pattern*, $N = 100$, $SLL = -20$ dB, $d = 0.5\lambda$, $L = 49.5\lambda$, $C = 21$)—Power pattern over the whole visible u−range (a) and a detail of the main lobe (b).
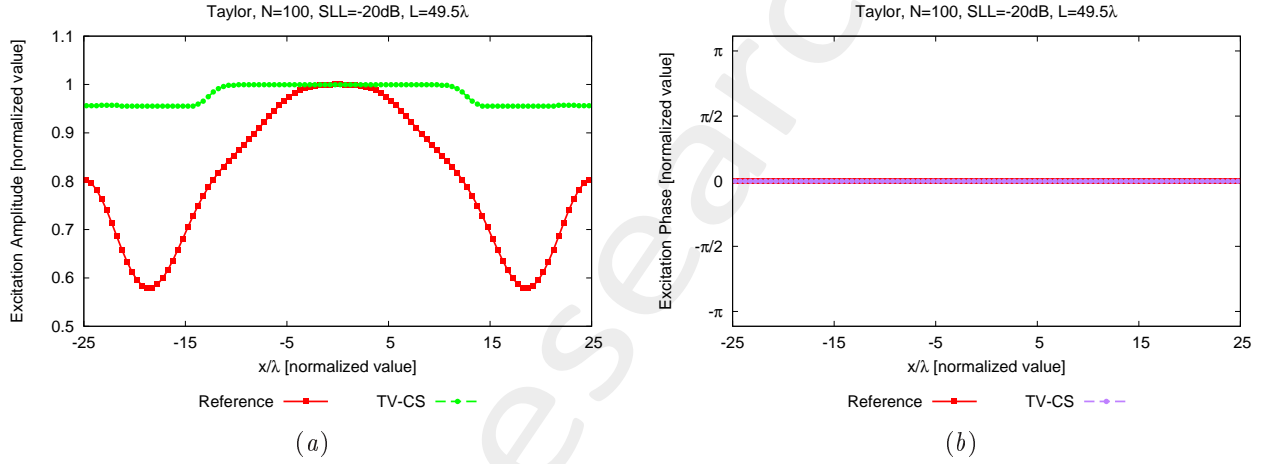

Figure 8: *Performance Assessment* (*Taylor Pattern*, $N = 100$, $SLL = -20$ dB, $d = 0.5\lambda$, $L = 49.5\lambda$, $C = 21$)—Excitations amplitude (a) and phase (b).
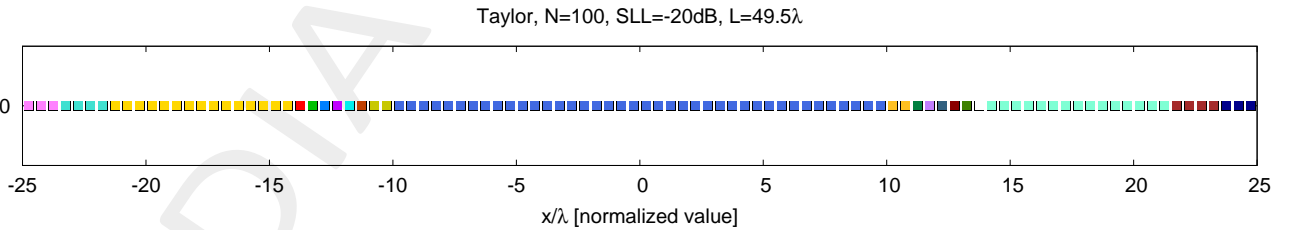

Figure 9: *Performance Assessment* (*Taylor Pattern*, $N = 100$, $SLL = -20$ dB, $d = 0.5\lambda$, $L = 49.5\lambda$, $C = 21$)—Array elements clustering configuration.

	C	SLL [dB]	BW [deg]	$D_{\max}$ [dB]	DRR_{max}[dB]	$\xi \left[\times 10^{-2} \right]$
Reference	−	−19.82	1.0842	19.87	2.37	−
$TV - CS$	21	−13.78	1.0222	19.99	0.20	2.20

Table III: *Performance Assessment* (*Taylor Pattern*, $N = 100$, $SLL = -20$ dB, $d = 0.5\lambda$, $L = 49.5\lambda$, $C = 21$)—Array Performance Indexes.

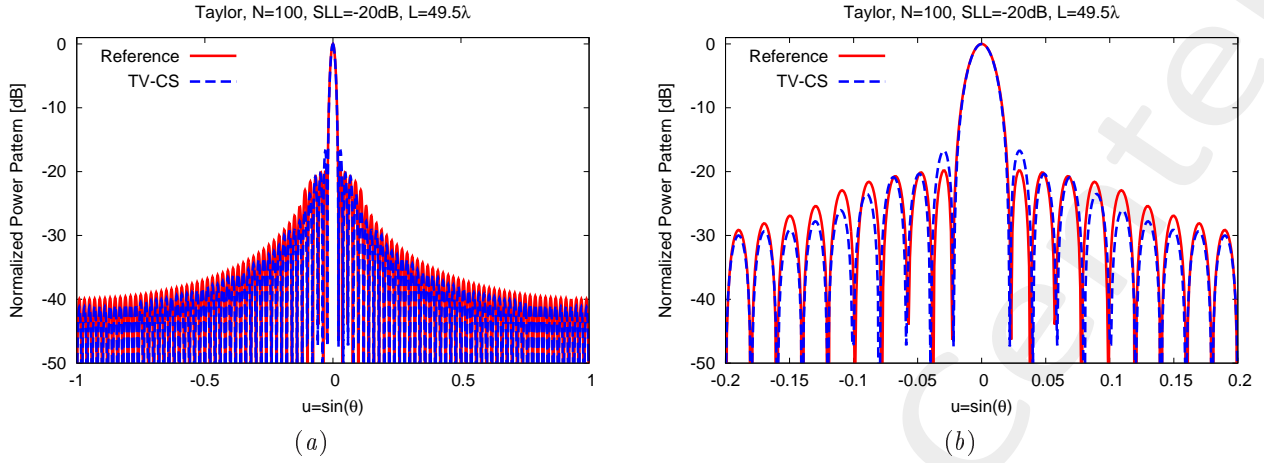**Number of Clusters:** $C = 39$

Figure 10: *Performance Assessment (Taylor Pattern, $N = 100$, $SLL = -20$ dB, $d = 0.5\lambda$, $L = 49.5\lambda$, $C = 39$)-*—Power pattern over the whole visible u—range (a) and a detail of the main lobe (b).
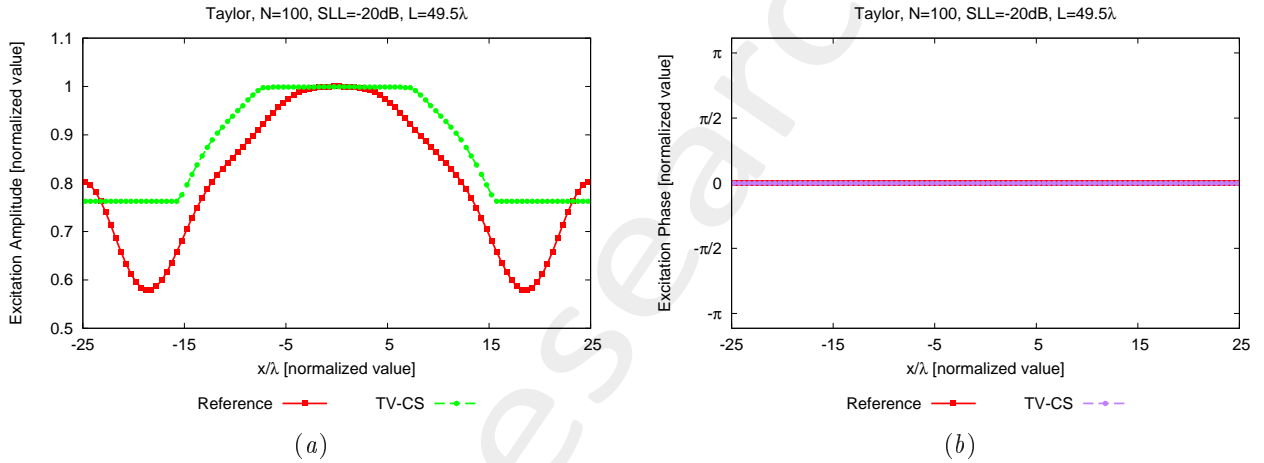

Figure 11: *Performance Assessment (Taylor Pattern, $N = 100$, $SLL = -20$ dB, $d = 0.5\lambda$, $L = 49.5\lambda$, $C = 39$)-*—Excitations amplitude (a) and phase (b).
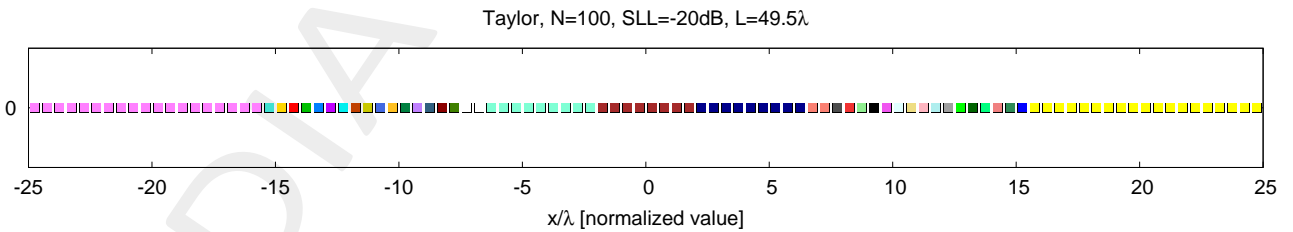

Figure 12: *Performance Assessment (Taylor Pattern, $N = 100$, $SLL = -20$ dB, $d = 0.5\lambda$, $L = 49.5\lambda$, $C = 39$)-*—Array elements clustering configuration.

	C	SLL [dB]	BW [deg]	$D_{\max}$ [dB]	DRR_{max}[dB]	$\xi \left[\times 10^{-3} \right]$
Reference	$-$	-19.82	1.0842	19.87	2.37	$-$
$TV-CS$	39	-16.73	1.0690	19.94	1.17	5.78

Table IV: *Performance Assessment (Taylor Pattern, $N = 100$, $SLL = -20$ dB, $d = 0.5\lambda$, $L = 49.5\lambda$, $C = 39$)-*—Array Performance Indexes.

Number of Clusters: $C = 53$

Taylor, N=100, SLL=-20dB, L=49.5λ

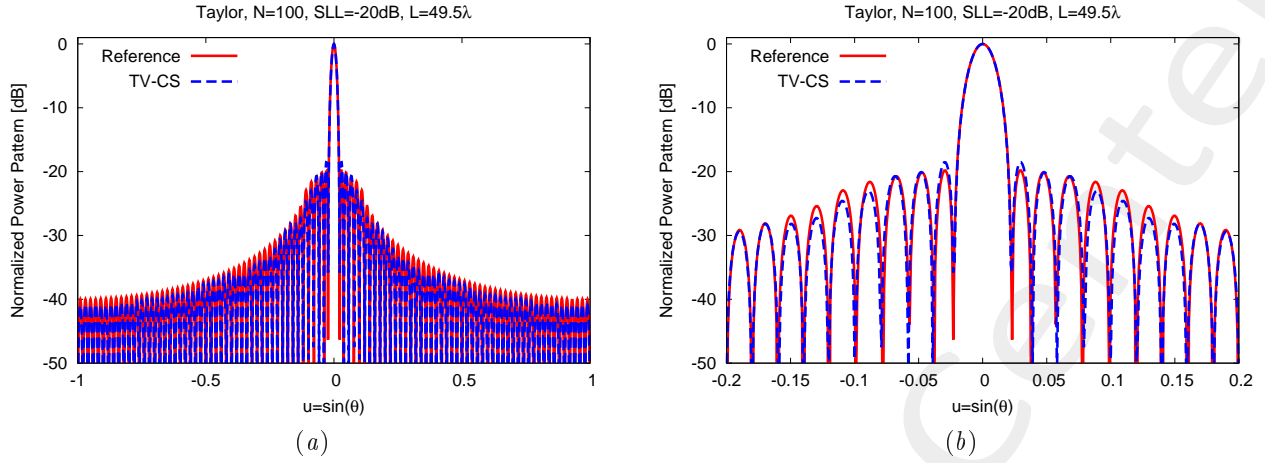(a)

Taylor, N=100, SLL=-20dB, L=49.5λ

(b)

Figure 13: *Performance Assessment (Taylor Pattern, $N = 100$, $SLL = -20$ dB, $d = 0.5\lambda$, $L = 49.5\lambda$, $C = 53$)-* —Power pattern over the whole visible $u-$range (a) and a detail of the main lobe (b).

Taylor, N=100, SLL=-20dB, L=49.5λ

(a)

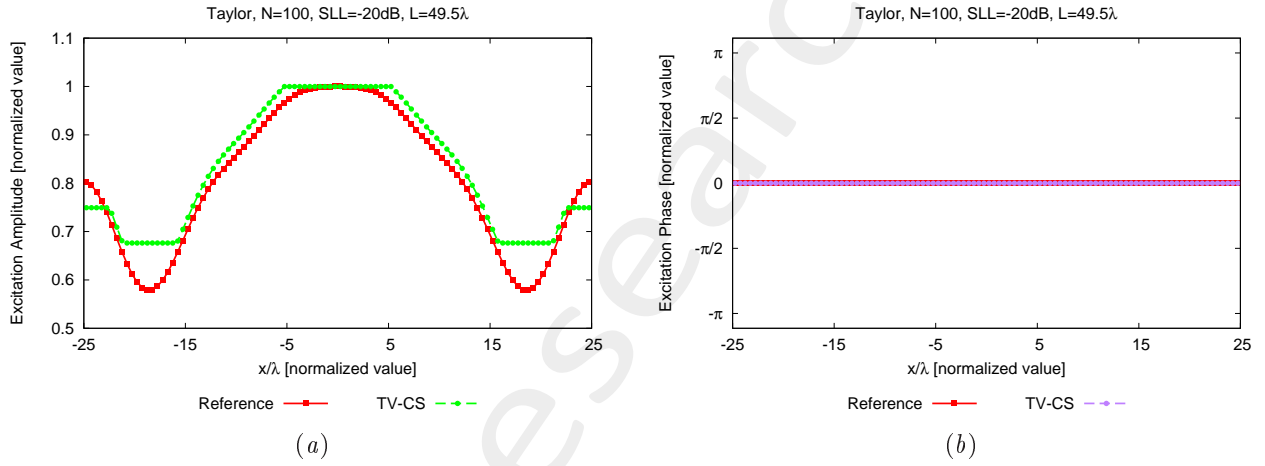Taylor, N=100, SLL=-20dB, L=49.5λ

(b)

Figure 14: *Performance Assessment (Taylor Pattern, $N = 100$, $SLL = -20$ dB, $d = 0.5\lambda$, $L = 49.5\lambda$, $C = 53$)-* —Excitations amplitude (a) and phase (b).
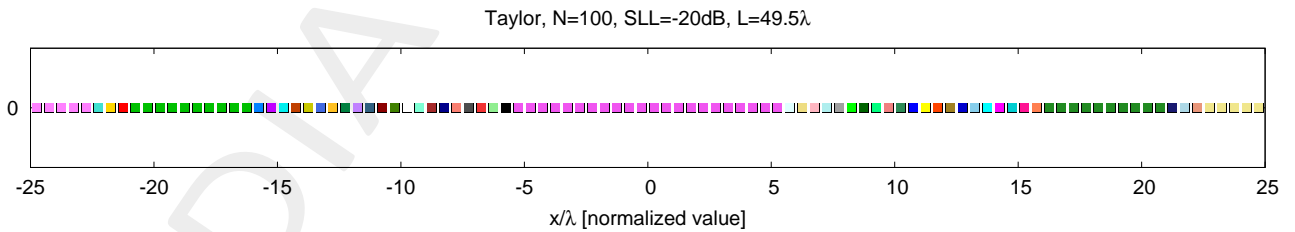

Taylor, N=100, SLL=-20dB, L=49.5λ

Figure 15: *Performance Assessment (Taylor Pattern, $N = 100$, $SLL = -20$ dB, $d = 0.5\lambda$, $L = 49.5\lambda$, $C = 53$)-* —Array elements clustering configuration.

	C	SLL [dB]	BW [deg]	$D_{\max}$ [dB]	DRR_{max}[dB]	$\xi \left[\times 10^{-3}\right]$
$Reference$	$-$	-19.82	1.0842	19.87	2.37	$-$
$TV - CS$	53	-18.54	1.0811	19.90	1.70	1.59

Table V: *Performance Assessment (Taylor Pattern, $N = 100$, $SLL = -20$ dB, $d = 0.5\lambda$, $L = 49.5\lambda$, $C = 53$)-* —Array Performance Indexes.
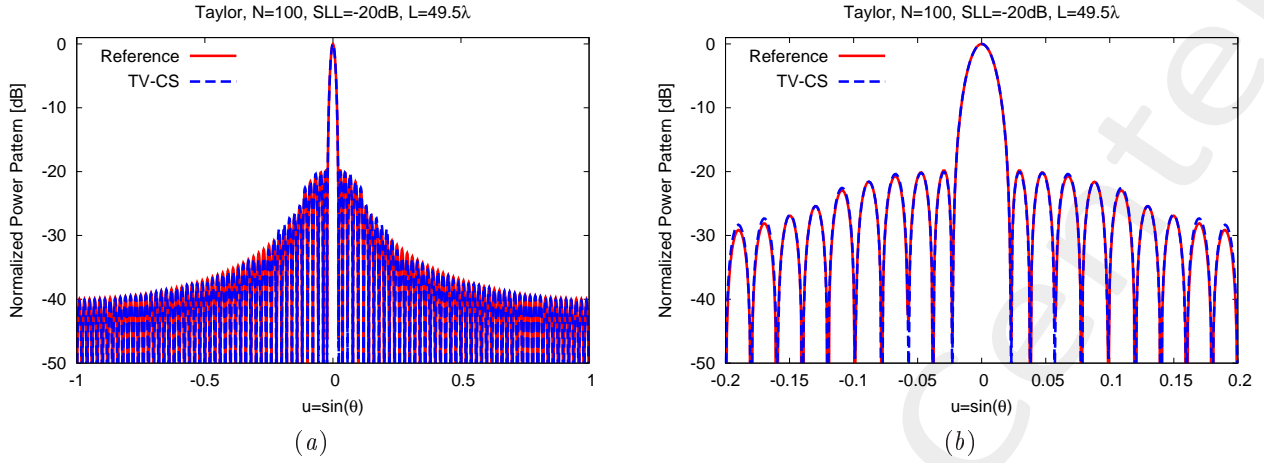
Number of Clusters: $C = 67$

Figure 16: *Performance Assessment* (*Taylor Pattern*, $N = 100$, $SLL = -20$ dB, $d = 0.5\lambda$, $L = 49.5\lambda$, $C = 67$)-
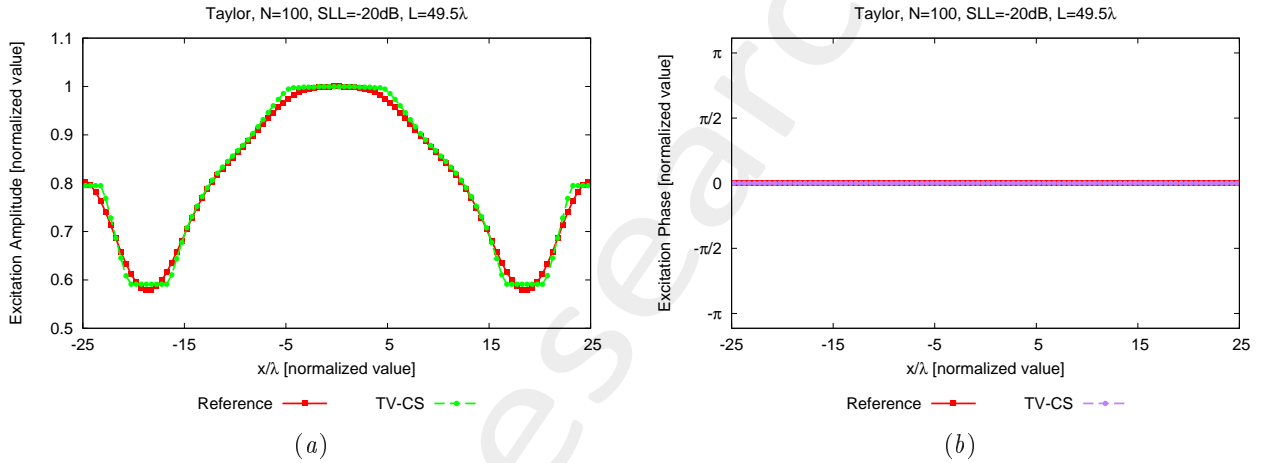—Power pattern over the whole visible u−range (a) and a detail of the main lobe (b).

Figure 17: *Performance Assessment* (*Taylor Pattern*, $N = 100$, $SLL = -20$ dB, $d = 0.5\lambda$, $L = 49.5\lambda$, $C = 67$)-
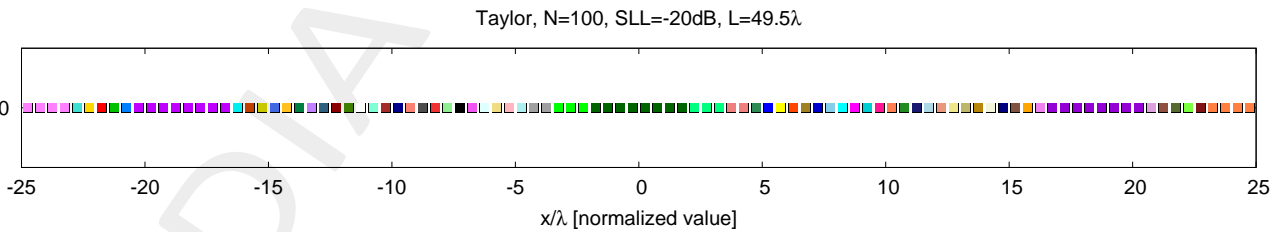—Excitations amplitude (a) and phase (b).

Figure 18: *Performance Assessment* (*Taylor Pattern*, $N = 100$, $SLL = -20$ dB, $d = 0.5\lambda$, $L = 49.5\lambda$, $C = 67$)-
—Array elements clustering configuration.

	C	SLL [dB]	BW [deg]	$D_{\max}$ [dB]	DRR_{max}[dB]	ξ $\left[\times 10^{-4}\right]$
Reference	−	−19.82	1.0842	19.87	2.37	−
$TV - CS$	67	−20.10	1.0852	19.86	2.28	1.97

Table VI: *Performance Assessment* (*Taylor Pattern*, $N = 100$, $SLL = -20$ dB, $d = 0.5\lambda$, $L = 49.5\lambda$, $C = 67$)-
—Array Performance Indexes.

RESULTS - TOLERANCE: $\tau_C = 1.0 \times 10^{-2}$

NOTE: With respect to the previous test cases the clustering "de-noise" tolerance has been decreased from $\tau_c = 1 \times 10^{-3}$ to $\tau_c = 1 \times 10^{-2}$, in order to avoid the problem noticed in the test case of Fig. 6, in which $C = 3$ clusters are counted, but watching Fig. 5 the array excitation distribution seems uniform.
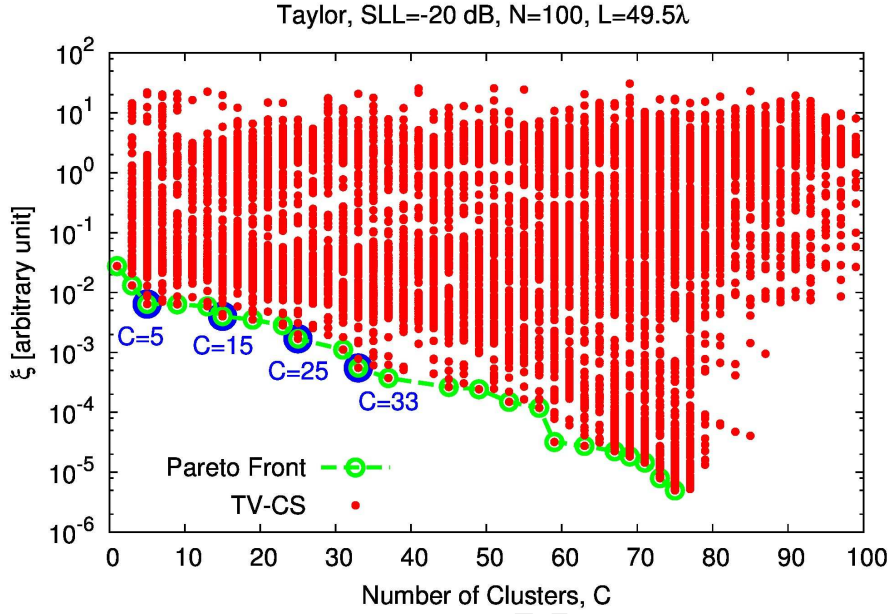
Pareto Front:

Figure 19: *Performance Assessment (Taylor Pattern, $N = 100$, $SLL = -20$ dB, $d = 0.5\lambda$, $L == 49.5\lambda$)*$-$Pareto front.

C	ξ	μ	β	K	m_t	m_o
5	6.43×10^{-3}	2×10^{-2}	2×10^{1}	60	2×10^{3}	5×10^{2}
15	4.00×10^{-3}	2×10^{-2}	2×10^{0}	90	1×10^{3}	5×10^{2}
25	1.69×10^{-3}	2×10^{-2}	2×10^{0}	90	2×10^{3}	5×10^{2}
33	5.53×10^{-4}	2×10^{-1}	5×10^{2}	200	5×10^{2}	5×10^{2}

Table VII: *Performance Assessment (Taylor Pattern, $N = 100$, $SLL = -20$ dB, $d = 0.5\lambda$, $L = 49.5\lambda$)*$-$Selected solutions.

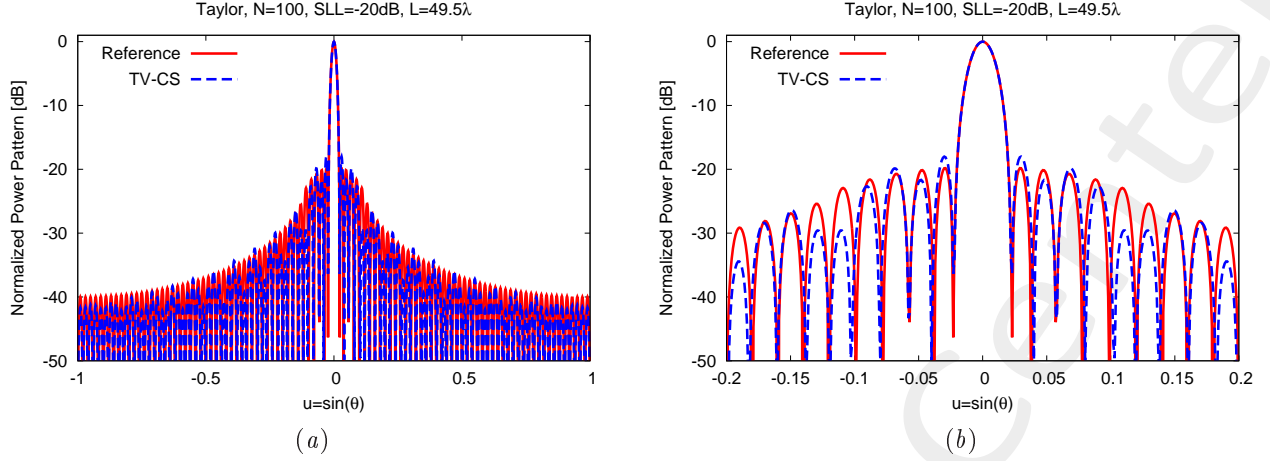**Number of Clusters:** $C = 5$

Figure 20: *Performance Assessment* (*Taylor Pattern*, $N = 100$, $SLL = -20$ dB, $d = 0.5\lambda$, $L = 49.5\lambda$, $C = 5$)--Power pattern over the whole visible u--range (a) and a detail of the main lobe (b).
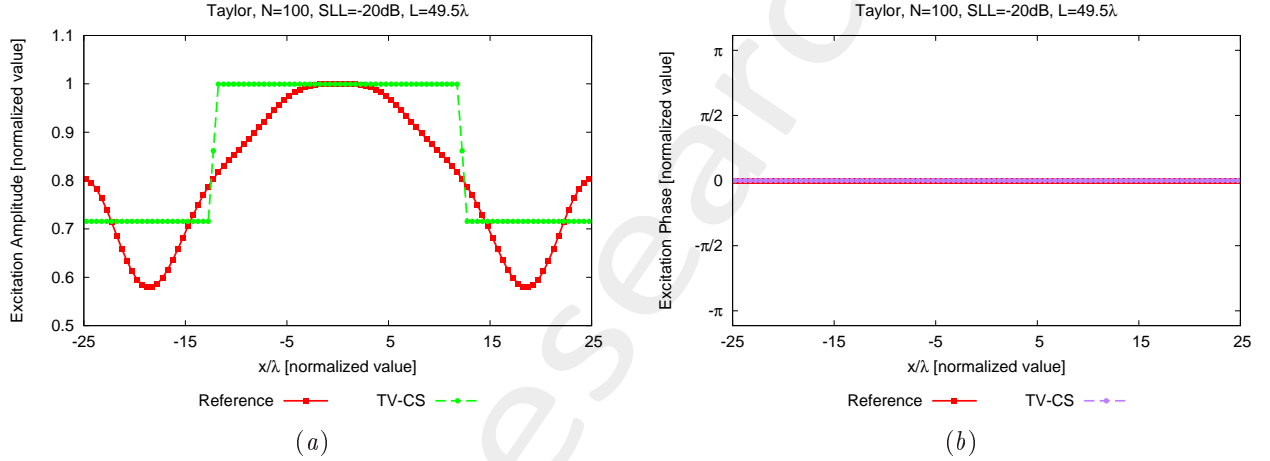

Figure 21: *Performance Assessment* (*Taylor Pattern*, $N = 100$, $SLL = -20$ dB, $d = 0.5\lambda$, $L = 49.5\lambda$, $C = 5$)--Excitations amplitude (a) and phase (b).
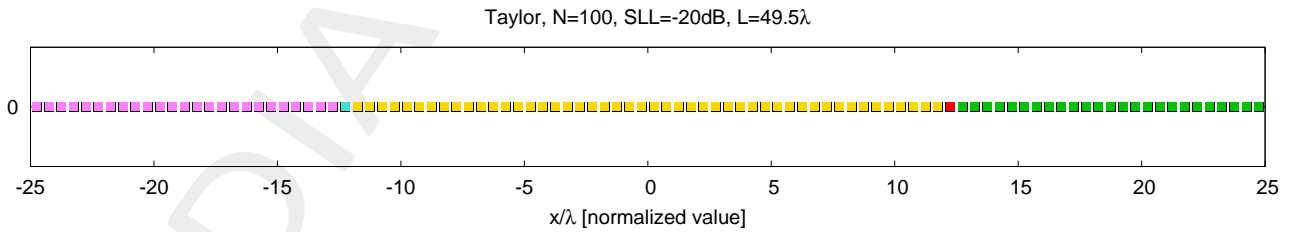

Figure 22: *Performance Assessment* (*Taylor Pattern*, $N = 100$, $SLL = -20$ dB, $d = 0.5\lambda$, $L = 49.5\lambda$, $C = 5$)--Array elements clustering configuration.

	C	SLL [dB]	BW [deg]	$D_{\max}$ [dB]	DRR_{max}[dB]	$\xi \left[\times 10^{-3} \right]$
Reference	$-$	-19.82	1.0842	19.87	2.37	$-$
$TV - CS$	5	-18.01	1.0868	19.88	1.45	6.42

Table VIII: *Performance Assessment* (*Taylor Pattern*, $N = 100$, $SLL = -20$ dB, $d = 0.5\lambda$, $L = 49.5\lambda$, $C = 5$)--Array Performance Indexes.

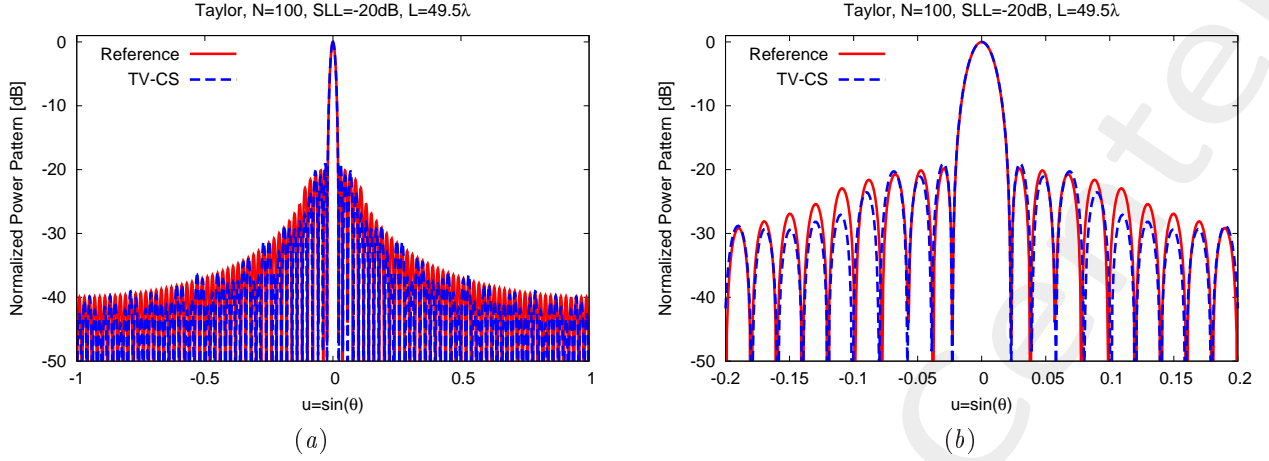**Number of Clusters:** $C = 15$

Figure 23: *Performance Assessment (Taylor Pattern, $N = 100$, $SLL = -20$ dB, $d = 0.5\lambda$, $L = 49.5\lambda$, $C = 15$)-*—Power pattern over the whole visible u−range (a) and a detail of the main lobe (b).
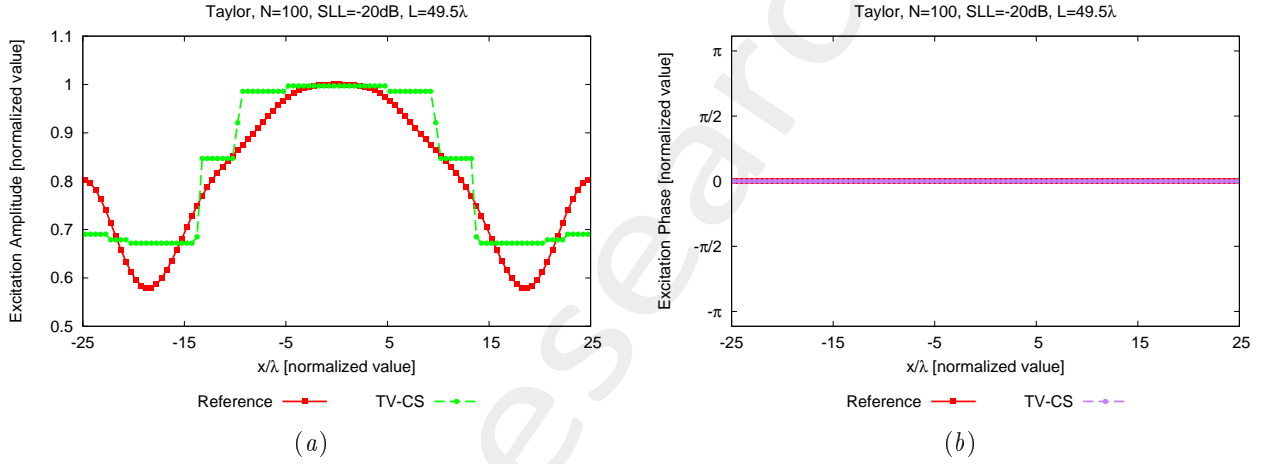

Figure 24: *Performance Assessment (Taylor Pattern, $N = 100$, $SLL = -20$ dB, $d = 0.5\lambda$, $L = 49.5\lambda$, $C = 15$)-*—Excitations amplitude (a) and phase (b).
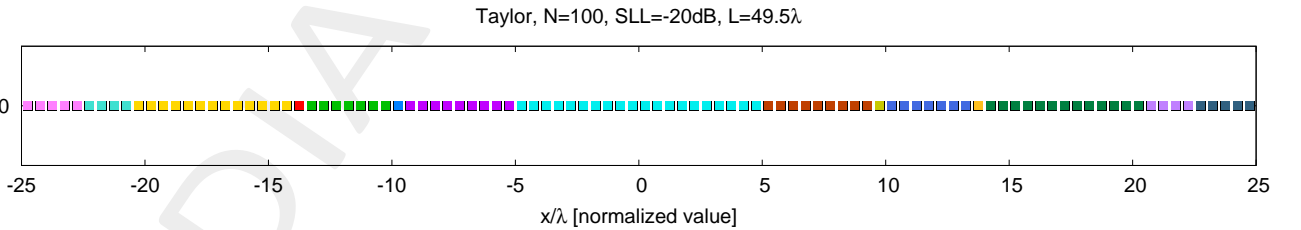

Figure 25: *Performance Assessment (Taylor Pattern, $N = 100$, $SLL = -20$ dB, $d = 0.5\lambda$, $L = 49.5\lambda$, $C = 15$)-*—Array elements clustering configuration.

	C	SLL [dB]	BW [deg]	$D_{\max}$ [dB]	DRR_{max}[dB]	ξ $[\times 10^{-3}]$
Reference	−	−19.82	1.0842	19.87	2.37	−
TV − CS	15	−19.02	1.1095	19.87	1.71	4.00

Table IX: *Performance Assessment (Taylor Pattern, $N = 100$, $SLL = -20$ dB, $d = 0.5\lambda$, $L = 49.5\lambda$, $C = 15$)-*—Array Performance Indexes.
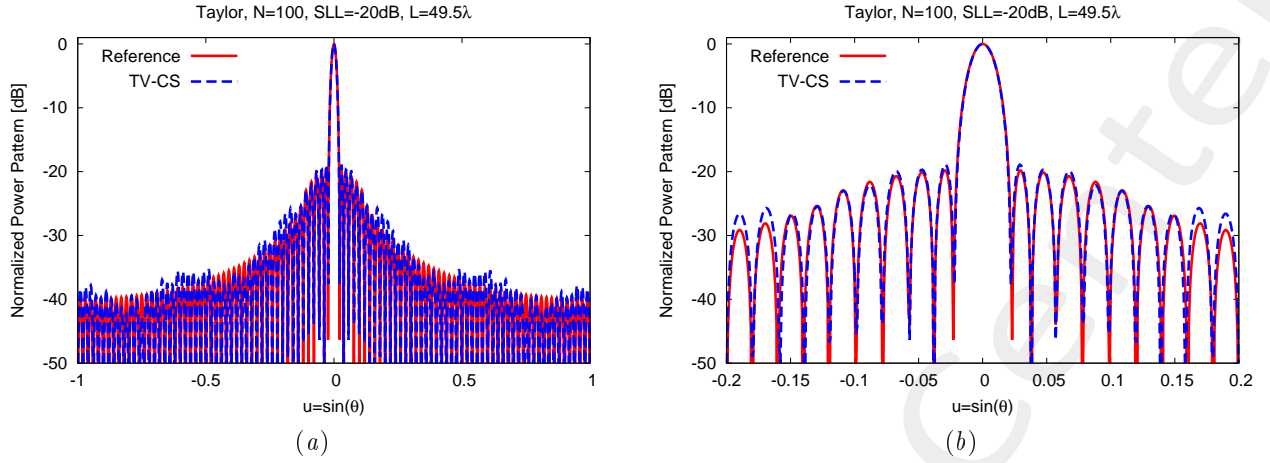
Number of Clusters: $C = 25$

Figure 26: *Performance Assessment (Taylor Pattern, $N = 100$, $SLL = -20$ dB, $d = 0.5\lambda$, $L = 49.5\lambda$, $C = 25$)- —Power pattern over the whole visible $u-$range (a) and a detail of the main lobe (b).*
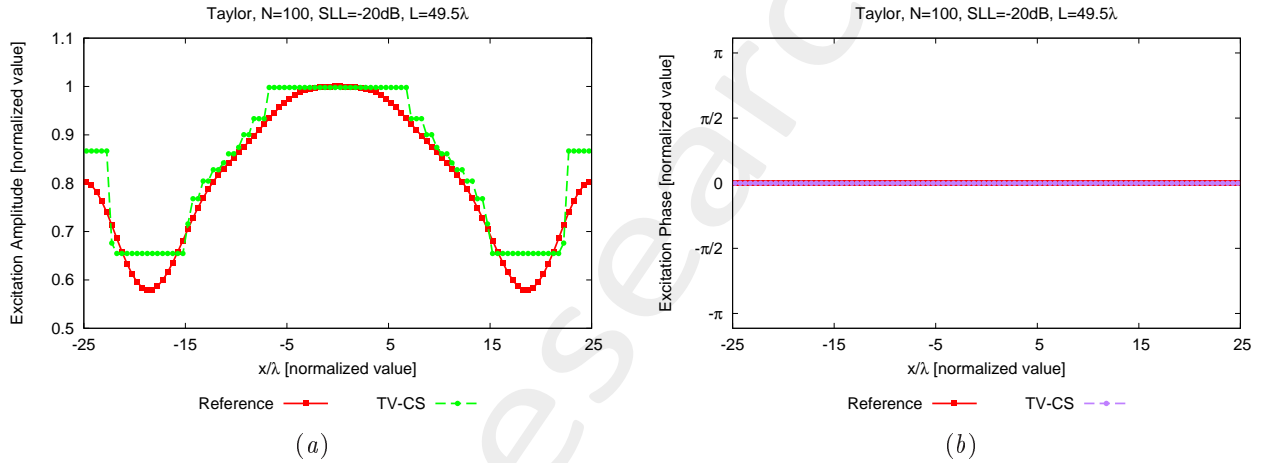

Figure 27: *Performance Assessment (Taylor Pattern, $N = 100$, $SLL = -20$ dB, $d = 0.5\lambda$, $L = 49.5\lambda$, $C = 25$)- —Excitations amplitude (a) and phase (b).*
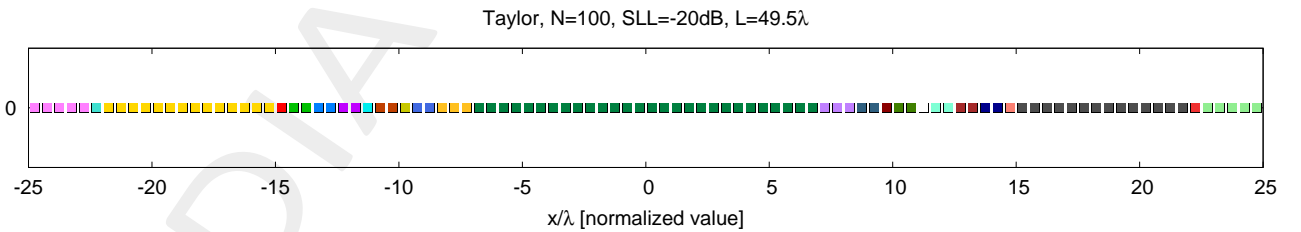

Figure 28: *Performance Assessment (Taylor Pattern, $N = 100$, $SLL = -20$ dB, $d = 0.5\lambda$, $L = 49.5\lambda$, $C = 25$)- —Array elements clustering configuration.*

	C	SLL [dB]	BW [deg]	$D_{\max}$ [dB]	DRR_{max}[dB]	ξ $\left[\times 10^{-3}\right]$
Reference	$-$	-20.10	1.0842	19.87	2.37	$-$
TV$-$CS	25	-18.69	1.0711	19.87	1.83	1.69

Table X: *Performance Assessment (Taylor Pattern, $N = 100$, $SLL = -20$ dB, $d = 0.5\lambda$, $L = 49.5\lambda$, $C = 25$)- —Array Performance Indexes.*
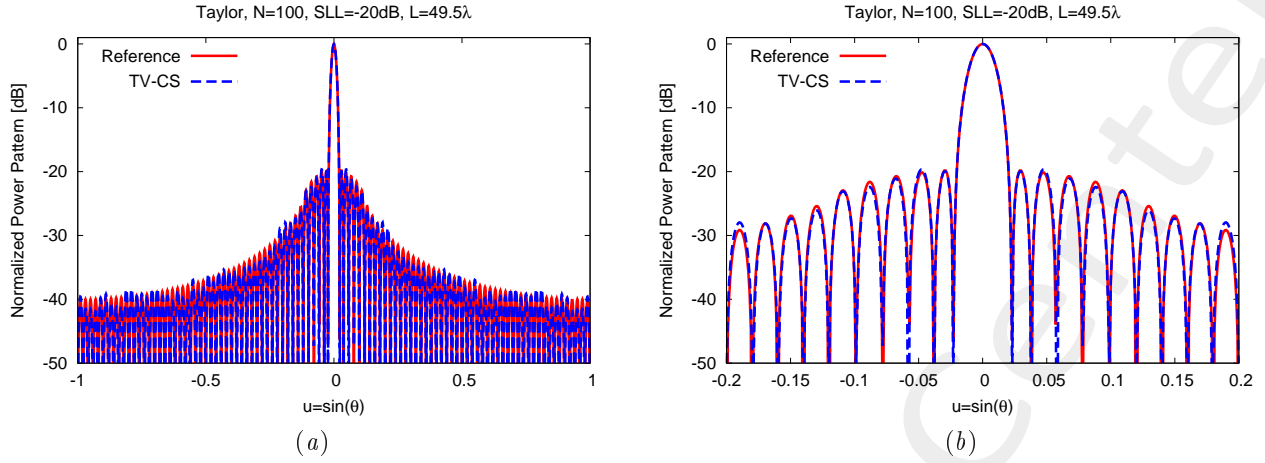
Number of Clusters: $C = 33$

Figure 29: *Performance Assessment (Taylor Pattern, $N = 100$, $SLL = -20$ dB, $d = 0.5\lambda$, $L = 49.5\lambda$, $C = 33$)-* —Power pattern over the whole visible u−range (a) and a detail of the main lobe (b).
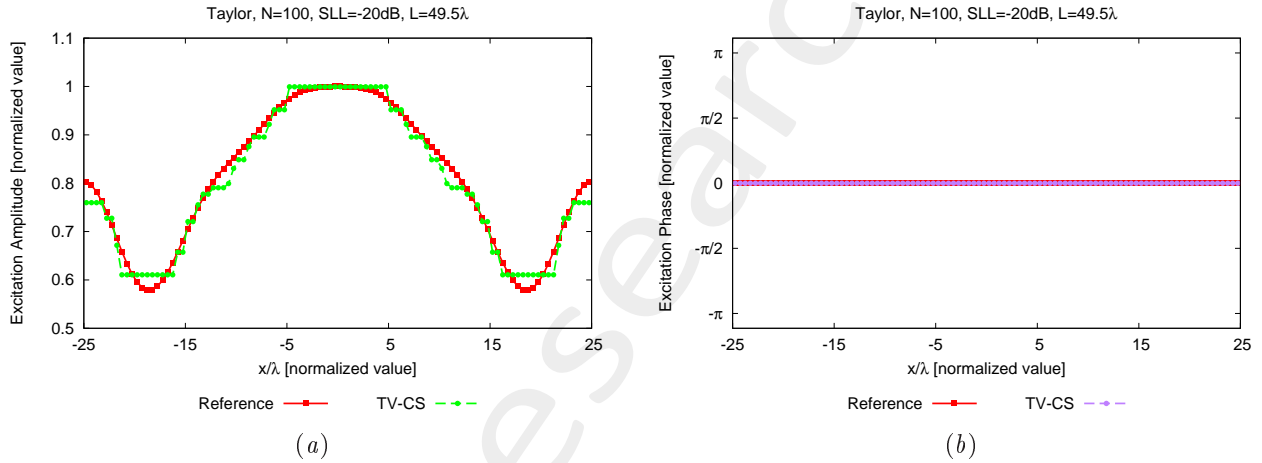

Figure 30: *Performance Assessment (Taylor Pattern, $N = 100$, $SLL = -20$ dB, $d = 0.5\lambda$, $L = 49.5\lambda$, $C = 33$)-* —Excitations amplitude (a) and phase (b).
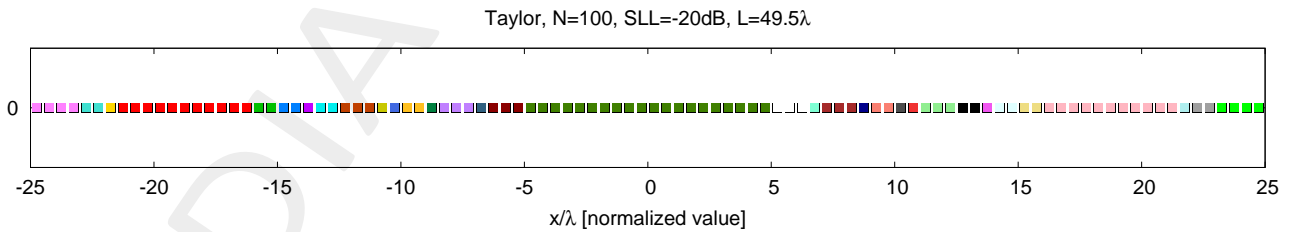

Figure 31: *Performance Assessment (Taylor Pattern, $N = 100$, $SLL = -20$ dB, $d = 0.5\lambda$, $L = 49.5\lambda$, $C = 33$)-* —Array elements clustering configuration.

	C	SLL [dB]	BW [deg]	$D_{\max}$ [dB]	DRR_{max}[dB]	$\xi \left[\times 10^{-4} \right]$
Reference	−	−20.10	1.0842	19.87	2.37	−
$TV - CS$	33	−19.66	1.0867	19.87	1.14	5.53

Table XI: *Performance Assessment (Taylor Pattern, $N = 100$, $SLL = -20$ dB, $d = 0.5\lambda$, $L = 49.5\lambda$, $C = 33$)-* —Array Performance Indexes.

4 Conclusions

This document presented an innovative $TV-CS$-based methodology for the synthesis of clustered linear arrays. Towards this end, the mathematical formulation of the linear array clustering problem, as well as its solution in a *sparseness*-regularized framework, has been described.

Some preliminary results have been shown in order to provide a first numerical assessment of the proposed strategy. From the reported outcomes it is possible to state that the proposed $TV-CS$ is able to synthesize sub-arrayed layouts consisting of a low number of clusters compared to the original elements, still guaranteeing a good matching of the reference pattern.

References

[1] P. Rocca, G. Oliveri, R. J. Mailloux, and A. Massa, "Unconventional phased array architectures and design methodologies - A Review," *Proc. IEEE*, vol. 104, no. 3, pp. 544-560, Mar. 2016.

[2] G. Oliveri, G. Gottardi, F. Robol, A. Polo, L. Poli, M. Salucci, M. Chuan, C. Massagrande, P. Vinetti, M. Mattivi, R. Lombardi, and A. Massa, "Co-design of unconventional array architectures and antenna elements for *5G* base stations," *IEEE Trans. Antennas Propag.*, vol. 65, no. 12, pp. 6752-6767, Dec. 2017.

[3] N. Anselmi, P. Rocca, M. Salucci, and A. Massa, "Irregular phased array tiling by means of analytic schemata-driven optimization," *IEEE Trans. Antennas Propag.*, vol. 65, no. 9, pp. 4495-4510, Sep. 2017.

[4] G. Oliveri, "Multi-beam antenna arrays with common sub-array layouts," *IEEE Antennas Wireless Propag. Lett.*, vol. 9, pp. 1190-1193, 2010.

[5] P. Rocca, R. Haupt, and A. Massa, "Sidelobe reduction through element phase control in sub-arrayed array antennas," *IEEE Antennas Wireless Propag. Lett.*, vol. 8, pp. 437-440, 2009.

[6] P. Rocca, L. Manica, R. Azaro, and A. Massa, "A hybrid approach for the synthesis of sub-arrayed monopulse linear arrays," *IEEE Trans. Antennas Propag.*, vol. 57, no. 1, pp. 280-283, Jan. 2009.

[7] G. Oliveri, P. Rocca, and A. Massa, "Reliable diagnosis of large linear arrays - a Bayesian compressive sensing approach," *IEEE Trans. Antennas Propag.*, vol. 60, no. 10, pp. 4627-4636, Oct. 2012.

[8] A. Massa, P. Rocca, and G. Oliveri, "Compressive sensing in electromagnetics - A review," *IEEE Antennas Propag. Mag.*, pp. 224-238, vol. 57, no. 1, Feb. 2015.

[9] G. Oliveri, M. Salucci, N. Anselmi, and A. Massa, "Compressive sensing as applied to inverse problems for imaging: theory, applications, current trends, and open challenges," *IEEE Antennas Propag. Mag.*, vol. 59, no. 5, pp. 34-46, Oct. 2017.

[10] P. Rocca, M. A. Hannan, M. Salucci, and A. Massa, "Single-snapshot DoA estimation in array antennas with mutual coupling through a multi-scaling Bayesian compressive sensing strategy," *IEEE Trans. Antennas Propag.*, vol. 65, no. 6, pp. 3203-3213, Jun. 2017.

[11] L. Poli, G. Oliveri, P. Rocca, M. Salucci, and A. Massa, "Long-distance WPT unconventional arrays synthesis," *J. Electromagn. Waves Appl.*, vol. 31, no. 14, pp. 1399-1420, Jul. 2017.

[12] G. Oliveri, M. Salucci, and A. Massa, "Synthesis of modular contiguously clustered linear arrays through a sparseness-regularized solver," *IEEE Trans. Antennas Propag.*, vol. 64, no. 10, pp. 4277-4287, Oct. 2016.

[13] F. Viani, G. Oliveri, and A. Massa, "Compressive sensing pattern matching techniques for synthesizing planar sparse arrays," *IEEE Trans. Antennas Propag.*, vol. 61, no. 9, pp. 4577-4587, Sept. 2013.

[14] G. Oliveri and A. Massa, "Bayesian compressive sampling for pattern synthesis with maximally sparse non-uniform linear arrays," *IEEE Trans. Antennas Propag.*, vol. 59, no. 2, pp. 467-481, Feb. 2011.

[15] N. Anselmi, G. Oliveri, M. A. Hannan, M. Salucci, and A. Massa, "Color compressive sensing imaging of arbitrary-shaped scatterers," *IEEE Trans. Microw. Theory Techn.*, vol. 65, no. 6, pp. 1986-1999, Jun. 2017.

[16] N. Anselmi, G. Oliveri, M. Salucci, and A. Massa, "Wavelet-based compressive imaging of sparse targets," *IEEE Trans. Antennas Propag.*, vol. 63, no. 11, pp. 4889-4900, Nov. 2015.

[17] G. Oliveri, N. Anselmi, and A. Massa, "Compressive sensing imaging of non-sparse 2D scatterers by a total-variation approach within the Born approximation," *IEEE Trans. Antennas Propag.*, vol. 62, no. 10, pp. 5157-5170, Oct. 2014.

[18] N. Anselmi, G. Gottardi, G. Oliveri, and A. Massa, "A total-variation sparseness-promoting method for the synthesis of contiguously clustered linear architectures" *IEEE Trans. Antennas Propag.*, vol. 67, no. 7, pp. 4589-4601, Jul. 2019.

[19] M. Salucci, A. Gelmini, G. Oliveri, and A. Massa, "Planar arrays diagnosis by means of an advanced Bayesian compressive processing," *IEEE Tran. Antennas Propag.*, vol. 66, no. 11, pp. 5892-5906, Nov. 2018.